ADVANCED MATERIALS INTERFACES
www.advmatinterfaces.de

Spontaneous Formation of Nanogap Electrodes by Self-Peeling Adhesion Lithography

*Sihai Luo, Bård H. Hoff, and John C. deMello**

Adhesion lithography ("a-lith") is a simple method for forming nanoscale gaps between dissimilar metals. In its usual form, a metal is patterned on a substrate, and conformally coated with an alkyl-functionalized self-assembled monolayer, rendering it nonadhesive to other metals; a second metal is then deposited uniformly over the full area of the substrate; finally, the parts of the second metal that are in contact with the self-assembled monolayer are stripped away using an adhesive tape or film, leaving the first and second metals side-by-side on the substrate, with a nanoscale spacing between them. It is shown here that, by depositing onto the second metal an adhesive film with high internal strain, it is possible to induce spontaneous delamination of the peeling layer without the need for any applied force. The modified procedure simplifies implementation and eliminates external stresses that can cause unwanted widening of the gap. The resultant electrode separations of ≈10 nm are amongst the smallest values achieved to date using adhesion lithography.

1. Introduction

Laterally aligned metal electrodes, separated on the nanometer length scale, are essential building blocks for nanoscale photonic and electronic devices.[1–4] Many methods for fabricating such electrodes have been reported, including mechanical break junctions,[5,6] electron-beam patterning,[7,8] atomic force and scanning probe lithographies,[9–11] focused ion beam milling,[12,13] on-wire lithography,[14,15] electromigration and electrochemical deposition,[16,17] nanosphere templating,[18,19] and atomic layer lithography.[20,21] Such methods, however, impose considerable trade-offs in terms of processing time, scalability, feature size, and equipment costs, which heavily restrict their use and accessibility[1,22,23] In addition, some methods leave hard-to-remove insulators in the "gap" region, preventing infilling of the gap by photonic or electronic materials; while others are limited to the patterning of a single metal, and consequently cannot be applied to the fabrication of asymmetric nanoscale devices such as rectifiers and ambipolar devices that require the use of closely spaced dissimilar metal electrodes.

Beesley et al. recently reported an alternative method for fabricating arrays of high aspect-ratio asymmetric nanogap electrodes, which exploits the ability of selected self-assembled monolayers (SAMs) to attach conformally to a prepatterned metal layer and thereby weaken adhesion to a subsequently deposited metal film.[24] The method—referred to as adhesion lithography or "a-lith"—has the advantage of involving only a few simple processing steps that can be carried out at room temperature under ambient conditions, using inexpensive equipment. Adhesion lithography provides a rapid route to highly aligned, electrically isolated, asymmetric electrodes separated on the nanometer length scale, and has been successfully applied to a broad range of nanogap devices, including light-emitting diodes,[25] optical sensors,[26] high frequency (>20 MHz) Schottky diodes,[27,28] field effect transistors,[29,30] and memristors.[30,31]

The main processing steps in the usual a-lith procedure are summarized in **Figure 1**. A thin (≈50 nm) metal film (M1) is deposited on a substrate, and selectively patterned to expose the underlying substrate in regions where a second metal will subsequently be deposited (Figure 1a). An alkyl-containing metallophilic SAM is conformally attached to all exposed surfaces of M1, with the alkyl chains facing outwards from the metal surface (Figure 1b). Next, a second metal film (M2) is uniformly deposited over the full area of the substrate (Figure 1c). Owing to the presence of the SAM, the adhesion of M2 to M1 is much weaker than its adhesion to the substrate. In consequence, if an adhesive tape or film is applied uniformly to the surface of M2 (Figure 1d) and then pulled away (Figure 1e-(i)), M2 will detach from the regions above M1 and remain only in those areas where M2 is in direct contact with the substrate. Hence, at the end of the procedure the two metals will sit in a complementary arrangement, side-by-side on the substrate, separated in the limiting case by just the length of the SAM—a few nanometers or less. The SAM may subsequently be removed by UV/ozone or oxygen plasma treatment, leaving an unfilled gap between the two electrodes (Figure 1f).

In practice, the reported electrode spacings achieved with adhesion lithography have been substantially higher than the SAM length, typically lying in the 15–100 nm size range, depending on how the peeling step is carried out. (Factors such

S. Luo, Prof. B. H. Hoff, Prof. J. C. deMello
Department of Chemistry
Norwegian University of Science and Technology (NTNU)
NO-7491 Trondheim, Norway
E-mail: john.demello@ntnu.no

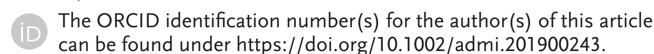
The ORCID identification number(s) for the author(s) of this article can be found under https://doi.org/10.1002/admi.201900243.

DOI: 10.1002/admi.201900243

© 2019 WILEY-VCH Verlag GmbH & Co. KGaA, Weinheim

ADVANCED MATERIALS INTERFACES
www.advmatinterfaces.de

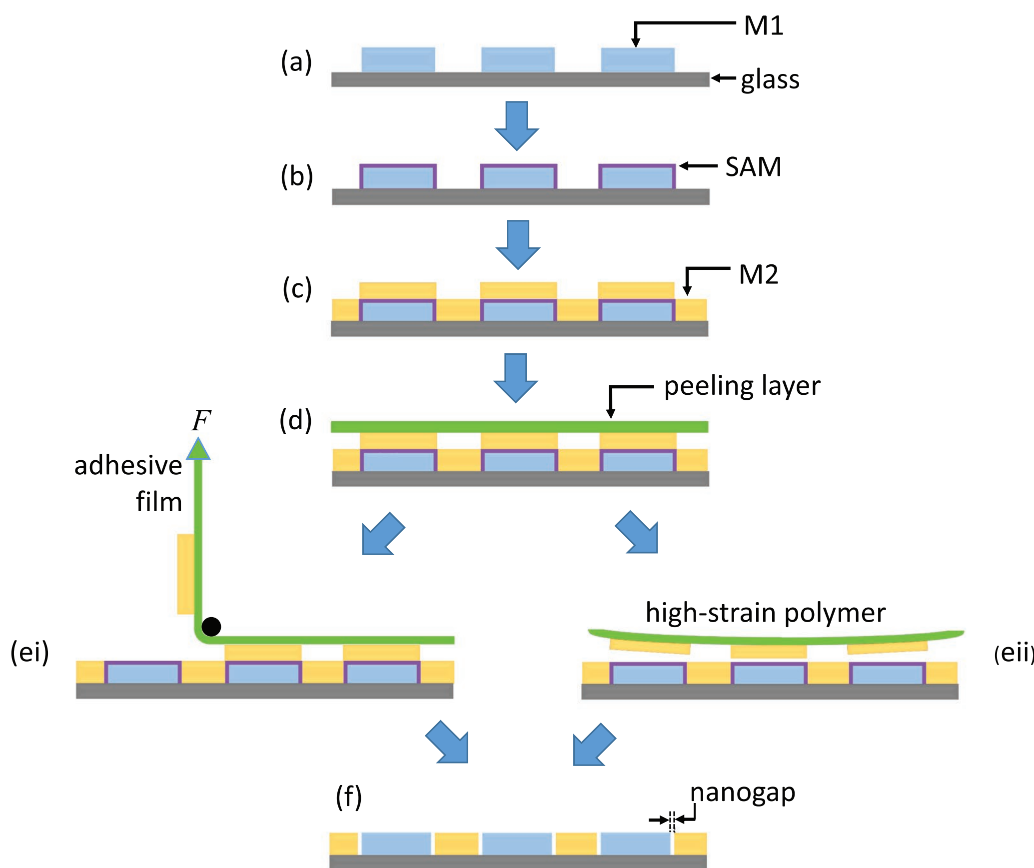

Figure 1. Schematic showing key processing steps in conventional and self-peeling adhesion lithography. The conventional procedure comprises the following steps: first, metal M1 is deposited on a substrate and patterned as appropriate (a); second, M1 is selectively coated with a metallophilic SAM (b); third, metal M2 is deposited uniformly over M1 and the exposed substrate (c); fourth, adhesive tape—or an alternative adhesive material—is applied to the surface of M2 (d); fifth, the tape is peeled away from the substrate, selectively removing M2 from those regions located directly above the SAM (ei); finally, the SAM is removed by UV/ozone or O_2-plasma treatment, leaving M1 and M2 sitting in a complementary arrangement side-by-side on the substrate (f), separated in the limiting case by the length of the SAM. The selfpeeling procedure follows the conventional method up to step (d), except the peeling layer comprises a polymer with a high coefficient of thermal expansion, spin-coated onto M2 from a heated solution. As the polymer film cools, tension builds inside the film until it is sufficient to induce spontaneous peeling of the polymer from the coated substrate, taking with it those parts of M2 that are located directly above the SAM (eii). The SAM is removed as before by UV/ozone or O_2-plasma treatment.

as the topographies of M1 and M2, the relative adhesive forces between the various layers, mechanical stresses applied during peeling, and the tackiness and elasticity of the adhesive layer may all affect the observed gap width). Improvements to the standard procedure are therefore needed if the ultimate resolution limit of a-lith is to be reached.

It is already known that small changes in methodology can have a significant influence on the observed gap width. Beesley et al. for instance achieved a significant reduction in the gap width by changing the peeling layer from electrical insulation tape to a solution-deposited thin-film polymer.[24] They noted that, while it was difficult to achieve gap widths below 100 nm using the tape, spacings of just a few tens of nanometers could be readily obtained using the polymer. They attributed the reduction in gap width to a lowering of the peak peeling force from 1.1 N for the tape to 0.35 N for the solution-deposited polymer, and speculated that additional reductions in gap width could be achieved by further lowering the peeling force.

Successful patterning by adhesion lithography requires the parts of M2 that lie above the SAM to be "split" from the parts of M2 that are in direct contact with the substrate; the former must be lifted away by the peeling layer, while the latter must remain on the substrate. To effect the split, it is necessary to overcome the cohesive forces that exist between the M2 metal atoms at the intended "break-lines." Interestingly, imaging of the surface of freshly-deposited M2 by atomic force microscopy (AFM) has previously revealed the existence of sharp fracture lines that follow the edge profile of M1, suggesting the necessary split has occurred even before the peeling step is carried out.[24] If this is the case, the only forces that need to be overcome during the peeling step are the (vertical) adhesive forces at the SAM/M2 and M2/peeling-layer interfaces. Hence, by carefully choosing the SAM and peeling layer materials, it should be possible to minimize the required peeling force and thereby avoid external stresses that would lead to inadvertent gap widening.

The peeling force F required to separate an adhering layer of thickness t and width w from a rigid surface (see **Figure 2**a) may be expressed in terms of the interfacial adhesion strength γ and the internal stress U_R in the adhering layer. Following Croll,[32]

© 2019 WILEY-VCH Verlag GmbH & Co. KGaA, Weinheim

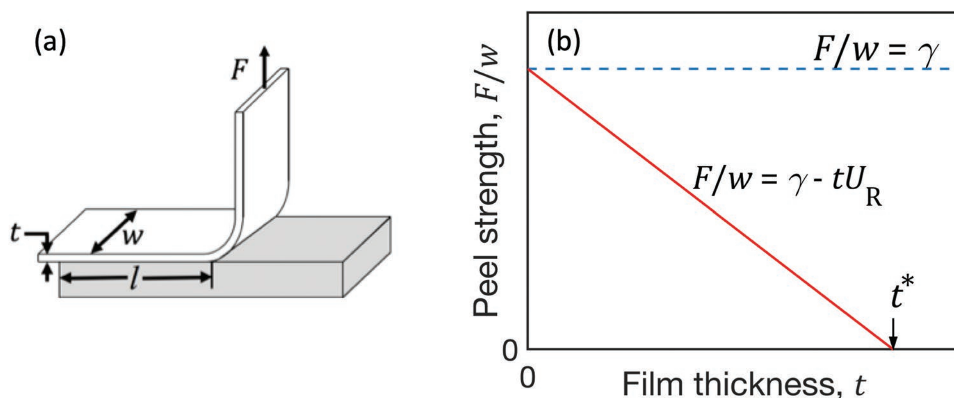

Figure 2. Force required to peel a thin film from a rigid substrate. a) Schematic showing a thin-film of thickness t, width w and contact length l being peeled from a rigid surface under an applied vertical force F. b) Graph showing the peel strength F/w versus t in an idealized system where the peel strength is governed by the interfacial strength of adhesion γ and the recoverable (volumetric) strain energy in the adhered film U_R. The peel strength decreases linearly from a value of γ at vanishingly low film thickness to a value of zero at a critical thickness $t^* = \gamma/U_R$. Films of thickness t^* and above detach spontaneously from the substrate without the need for any applied force.

if a short length of the adhering layer is peeled away from the surface—reducing the contact length from l_0 to l—then the total energy U_T of the system may be written as

$$U_T = \gamma w(l_0 - l) + lwtU_R - F(l_0 - l) \quad (1)$$

The first term on the right-hand side denotes the energy expended in forming the separated surfaces; the second term denotes the recoverable strain energy stored in the part of the coating that is still attached, assuming the internal strain is constant throughout the thickness of the coating; and the third term represents the change in the potential energy of the applied force. Conservation of energy during the peeling process implies $dU_T/dl = 0$, from which it follows that

$$\frac{F}{w} = \gamma - tU_R \quad (2)$$

Hence, the peel strength F/w required to remove the layer from the substrate is equal to the interfacial adhesion strength γ only when there is no strain in the adhered film, i.e., $U_R = 0$. The effect of strain is to lower the peel strength by an amount tU_R (see Figure 2b), making it easier to detach the adhering layer from the surface. Indeed, if the film thickness exceeds a critical value $t^* = \gamma/U_R$, the peel strength reduces to zero, causing the film to detach spontaneously from the surface without the need for any applied force.

Here, we exploit the self-peeling effect to develop a modified version of a-lith that we refer to as self-peeling adhesion lithography. We show that the modified procedure retains the key advantages of the original a-lith method, while at the same time simplifying implementation and improving reliability.

2. Results and Discussion

To make use of the self-peeling effect in adhesion lithography, a single layer of the adhesive material must detach spontaneously from those parts of M2 that are in direct contact with the substrate, leaving M2 attached to the substrate; while, everywhere else, a bilayer of M2 and the peeling layer must detach from the SAM, leaving the SAM-coated metal M1 exposed. For this to occur in a controlled and reliable manner, three peeling criteria must be satisfied: (i) the recoverable strain energy per unit area in the peeling layer must exceed the strength of adhesion at both the SAM/M2 and M2/peeling layer interfaces to ensure that spontaneous detachment can occur across the entire substrate; (ii) the adhesive strength between the peeling layer and M2 must be substantially weaker than the adhesive strength between M2 and the substrate to prevent accidental removal of M2 from the substrate; and (iii) the adhesive strength between the peeling layer and M2 must be stronger than the adhesive strength between M2 and the SAM to ensure complete removal of M2 from the SAM.

Following Beesley et al., for the work that follows we use aluminum as the first metal (M1), gold as the second metal (M2), and octadecylphosphonic acid (ODPA) as the SAM due to its ability to attach conformally and firmly to lightly oxidized aluminum.[24] To meet the first peeling criterion, we select as our peeling layer the thermoplastic fluoropolymer polyvinylidene fluoride (PVDF), which is characterized by a very high coefficient of thermal expansion α of more than 10^{-4} K^{-1} and a high Young's modulus E of more than 8 GPa.[33] The modified procedure follows the original method up to step (d), except the peeling layer is a ≈4 µm layer of PVDF spin-cast from a heated solution (N,N-dimethylformamide (DMF), 80 °C), see Experimental Section. In cooling to room temperature, an unconstrained film of PVDF would undergo a volumetric contraction of order one percent ($\Delta V/V = \alpha\Delta T$). However, as a result of being adhered to the metal-coated substrate, contraction of the PVDF is prevented, causing the constituent bonds to be stretched beyond their equilibrium values. Owing to the high Young's modulus of PVDF, significant stress builds inside the PVDF layer upon cooling, which as we show below is sufficient to induce spontaneous peeling at both the ODPA/Au and Au/PVDF interfaces.

To ensure the second and third peeling criteria are met, an ultrathin film of an oxidative metal (Al, 5 nm) is deposited

© 2019 WILEY-VCH Verlag GmbH & Co. KGaA, Weinheim

before gold evaporation to improve its adhesion to glass, and the adhesion between the PVDF layer and gold is tuned to a suitable level by carefully selecting the deposition and annealing conditions. Allowing the substrate to cool passively to room temperature after spin-casting the PVDF layer from an 80 °C solution has been found to deliver acceptable results in most cases. (The influence of the annealing conditions on the adhesion between PVDF and Au—and the "knock-on" effect on the patterning fidelity—are discussed in Figures S1–S4 in the Supporting Information).

Using the above conditions, uniform layers of aluminum (50 nm), gold (45 nm), and PVDF (≈4 µm) were sequentially deposited onto borosilicate glass substrates, with and without a monolayer of ODPA between the aluminum and gold. (In the former case an ultrathin layer of aluminum was deposited prior to gold deposition. References to "gold" in the text that follows should be understood to include an ultrathin Al adhesion layer on the underside).

With ODPA present (**Figure 3**a), a bilayer of gold and PVDF peeled away from the ODPA as the stack cooled (Figure 3b), leaving a (gold-free) continuous layer of ODPA-coated aluminum on the substrate (Figure 3c). Without ODPA present (Figure 3d), the PVDF peeled cleanly from the gold surface with no metal residue visible on the film (Figure 3e), leaving a continuous gold/aluminum bilayer on the substrate (Figure 3f). From Figure 3b,c, it is clear that delamination at the ODPA/Au interface occurs in preference to delamination at the Au/PVDF interface (or indeed any other interface); while, from Figure 3e,f, it is evident that delamination at the Au/PVDF interface occurs in preference to delamination at the glass/metal interface. In both cases the recoverable strain energy in the PVDF peeling layer was evidently sufficient to induce delamination. Taking these observations together, we conclude that all three criteria for reliable patterning are satisfied by the selected set of materials. We further conclude that—during the self-peeling a-lith procedure—peeling will either occur at the ODPA/Au interface, leaving ODPA-coated Al exposed; or—if no ODPA is present at that location—it will occur at the Au/PVDF interface, leaving Au exposed.

Figure 4 shows an illustrative sequence of images, obtained at various stages in the modified a-lith procedure. In the first step, a substrate is photolithographically patterned with aluminum, yielding an array of concentrically patterned circles (see Figure S5 in the Supporting Information for mask design). The patterned substrate is cleaned in oxygen plasma, immersed in an isopropanol-based solution of ODPA, and then rinsed lightly in isopropanol to remove unbound/residual SAM molecules, leaving a substrate patterned with ODPA-coated aluminum (Figure 4a). In the next step, the entire area of the substrate is evaporatively coated with a uniform layer of gold (Figure 4b). Then a ≈4 µm layer of PVDF is spin-coated on top of the gold from a heated solution (Figure 4c). The coated substrate is then allowed to cool under ambient conditions, causing the PVDF to peel spontaneously from the substrate and thereby strip away the parts of the gold film that are located directly above the patterned aluminum (Figure 4f). The gold and aluminum left behind on the substrate sit in a closely spaced side-by-side arrangement, separated in the limiting case by the width of an OPDA molecule, forming an array of filled nanogap electrodes (Figure 4d,e). In the final step (not shown), ODPA is

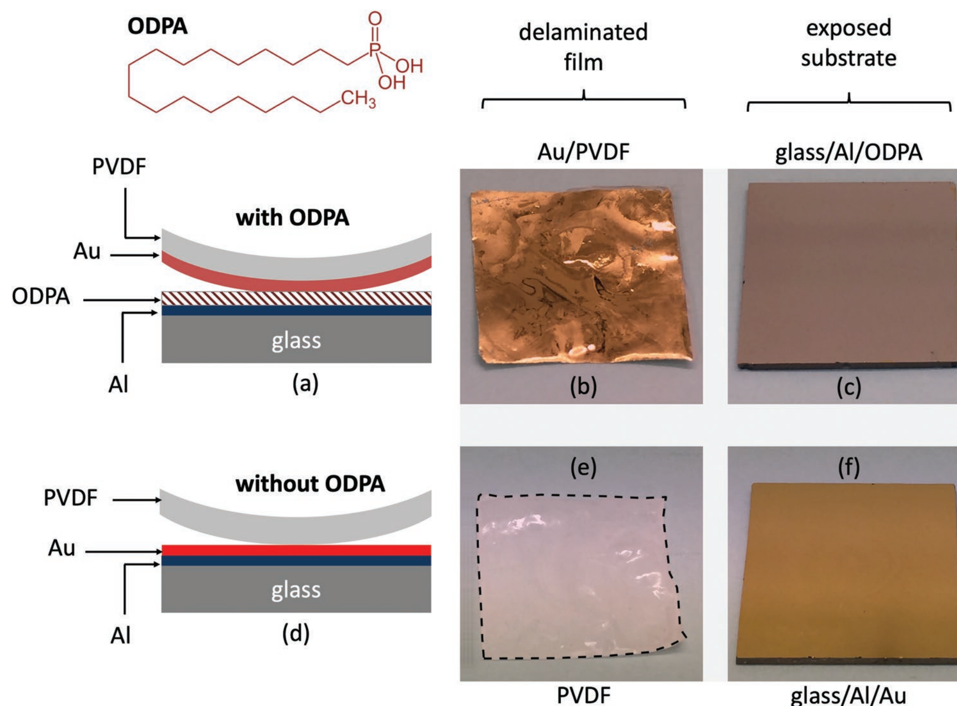

Figure 3. Images showing how the insertion of a self-assembled monolayer of octadecylphosphonic acid (ODPA) between thin-film aluminium (M1) and thin-film gold (M2) influences the peeling behaviour of PVDF. With ODPA present (a), a bilayer of gold and PVDF (b) delaminates cleanly from the stack, leaving ODPA-coated aluminium adhered to the glass substrate (c). In the absence of ODPA (d), a single layer of PVDF (e) delaminates cleanly from the metal-coated substrate (f).

© 2019 WILEY-VCH Verlag GmbH & Co. KGaA, Weinheim

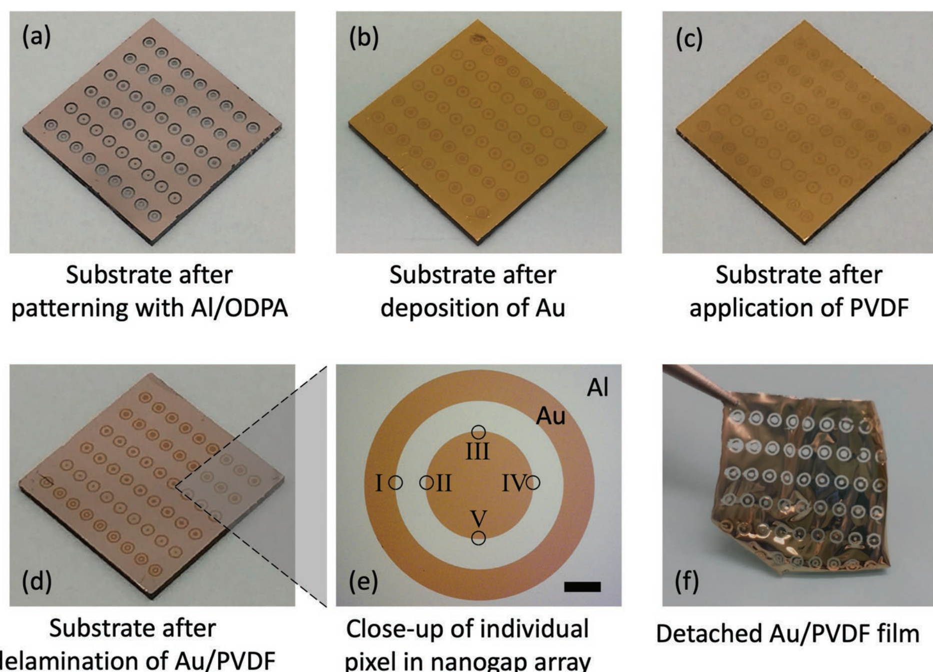

Figure 4. Series of photographs taken at each stage in the nanogap fabrication procedure. An array of ≈50-nm-thick aluminium electrodes (of varying design, see Figure S5) is lithographically patterned on top of a glass substrate, and conformally coated with ODPA (a); the entire substrate is coated with a ≈50 nm layer of gold (b); a ≈4-µm-layer of PVDF is spin-cast onto the gold from a heated (80 °C) solution in DMF (c); on cooling, the PVDF layer peels away from the coated substrate (f), taking with it those parts of the gold film that lie directly above the aluminium electrodes; at the end of the procedure, aluminium and gold sit side by side on the glass substrate (d), separated by a nanogap. A close-up of a single pixel from the nanogap array is shown in (e), with the small black circles denoting the approximate imaging regions for the SEM images in Figure 5.

removed from the aluminum by oxygen plasma treatment, leaving behind an array of open nanogap electrodes. (Similar images for symmetric Al/Al nanogap electrodes are shown in Figure S6 in the Supporting Information).

Figure 5 shows illustrative scanning electron microscopic (SEM) images obtained at the five approximate locations denoted in Figure 4e. Figure 5a shows a low magnification (×35 000) SEM image, recorded over a ≈4-µm-section of the nanogap, recorded at position I of Figure 4e. Despite the jagged edge profile of the pre-patterned Al electrode, the edge of the gold electrode closely tracks the edge of the aluminum (the first deposited metal), with a modal clearance of ≈10 nm (see histogram in Figure S7 in the Supporting Information). The tight nanogap is maintained over the full length of the image, except for a few sections where loss of gold from the glass substrate has caused a widening of the gap to a few tens of nanometers; the material loss is likely attributable to weakened gold adhesion caused by residual spots of ODPA on the glass. Figure 5b shows high magnification (×500 000) SEM images for the locations II, III, IV, and V of Figure 4e. Histograms of the electrode separation are shown adjacent to the images in Figure 5c. The data, derived from ≈40 measurements obtained at 7 nm intervals along the gap, indicate similar average electrode separations of ≈10 nm in each case. In contrast to data reported previously by Beesley et al. for mechanically induced peeling, the images suggest no significant variation of the gap width with direction.[24] The electrode spacings seen here are amongst the narrowest values so far reported for a-lith, suggesting the elimination of externally applied forces during the peeling step is an important requirement for maximizing the patterning resolution. It should be noted, however, that the observed gap widths are still substantially higher than the ≈2-nm-length of the ODPA molecule, indicating there is further scope for improvement through process optimization.

To confirm the suitability of the nanogap electrodes for electronic device applications, asymmetric Al/Au nanogap electrodes were fabricated as described above and the (insulating) ODPA layer was removed using an oxygen plasma. Electrical contact was made to the two electrodes, and the current (I) was measured as a function of the applied bias (V) over the range −0.5 to +0.5 V. Despite high applied field strengths of order 10^8 V m^{-1}, the measured current remained low (<15 pA) across the full sweep (see Figure S8 in the Supporting Information), confirming the good electrical (and physical) isolation of the asymmetric electrodes. Planar organic photodiodes were fabricated by depositing a layer of poly(3-hexylthiophene) (P3HT) uniformly over the nanogap electrodes. The photovoltaic (PV) response of the photodiodes was determined by carrying out current–voltage sweeps from −0.5 to +0.5 V at approximate illumination intensities of 0, 15, and 20 mW cm^{-2}. Well-behaved I–V curves were obtained in each case (see **Figure 6**a), with an approximately symmetric current–voltage response in the dark that varied from −34 ± 1 pA at −0.5 V to 29 ± 1 pA at +0.5 V, and photocurrents of ≈2 nA at −0.5 V.

The devices responded synchronously to pulsed illumination with rise and fall times of order 30 s (see Figure S9 in the Supporting Information)—similar to photovoltaic nanogap

© 2019 WILEY-VCH Verlag GmbH & Co. KGaA, Weinheim

Figure 5. Representative scanning electron microscopic images and corresponding spacing histograms for nanogap electrodes. a) Low magnification scanning electron microscopic image for a single ≈4-µm-section of a circular nanogap electrode, see position I of the pixel shown in Figure 4e. b) High magnification scanning electron microscopic images for four ≈280-nm-sections of a single circular nanogap electrode, see positions II–V of the pixel shown in Figure 4e. c) Spacing histograms extracted from the data in Figure 5b; each histogram was based on ≈40 measurements recorded at 7 nm intervals.

devices reported previously in the literature.[34,35] Equivalent devices fabricated with symmetric Al/Al electrodes exhibited an extremely weak photovoltaic response with currents less than 25 pA (see Figure 6b and Figure S10 (Supporting Information)), confirming the importance of being able to pattern asymmetric electrodes.[38]

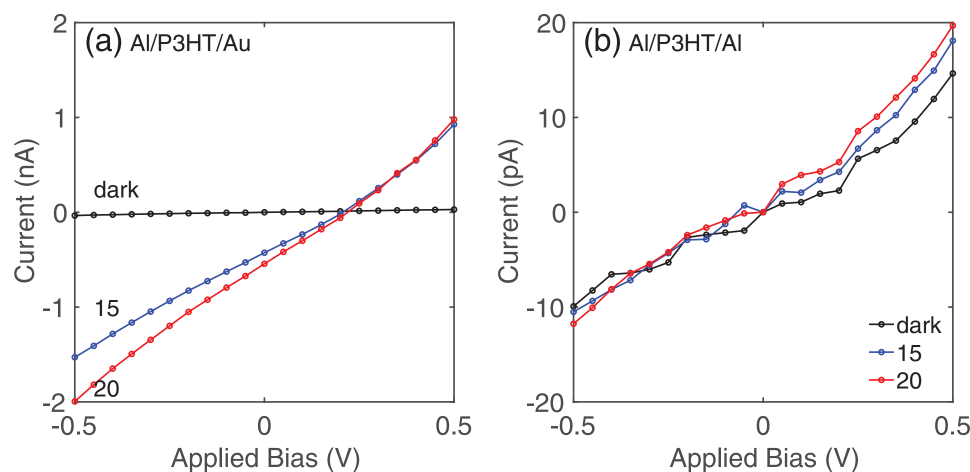

Figure 6. Electrical characterization of nanogap photodiodes. Current–Voltage curves for a) asymmetric Al/P3HT/Au and b) symmetric Al/P3HT/Al nanogap photodiodes, measured at approximate illumination intensities of 0, 15, and 20 mW cm^{-2}.

© 2019 WILEY-VCH Verlag GmbH & Co. KGaA, Weinheim

3. Conclusions

In conclusion, we have reported an adaptation of adhesion lithography that uses a thin-film polymer with high internal strain to induce spontaneous delamination of the peeling layer without the need for mechanical actuation. The revised procedure retains all of the advantages of standard adhesion lithography, e.g., the ability to pattern high-aspect-ratio asymmetric nanogap electrodes under ambient conditions without high cost deposition or alignment equipment. But additionally—by removing the need for a mechanically applied peeling force during delamination—it reduces the external stresses applied to the metal electrodes during peeling, and so helps avoid inadvertent widening of the nanogap. The resultant electrode separations of ≈10 nm show no significant directional variation and are amongst the smallest values achieved to date using adhesion lithography.

4. Experimental Section

Preparation of PVDF Solution: A 30 wt% mixture of PVDF (M_n = 71 000, Sigma-Aldrich) in *N*,*N*-dimethylformamide (DMF) solvent was prepared in a glass vial. The mixture was heated in a water bath at 80 °C and stirred magnetically at 1000 rpm for approximately four hours until a clear, homogeneous yellow solution was obtained.

Preparation of Al/Au/PVDF-Coated Glass Substrate: A 2 cm by 2 cm borosilicate glass substrate was cleaned and loaded into a high vacuum (10^{-6} mbar) e-beam evaporator, and 50 nm layers of Al and Au were sequentially deposited at 1.0 Ås^{-1}. The substrate was removed from the evaporator and dried on a hot plate at 80 °C for ten minutes. A PVDF layer was spin-cast on top of the gold layer from a heated solution (80 °C, 1000 rpm, 30 s). The substrate was then allowed to cool under ambient conditions for approximately three minutes to induce peeling of the PVDF layer at the Au/PVDF interface.

Preparation of Al/ODPA/Au/PVDF-Coated Glass Substrate: A 2 cm by 2 cm borosilicate glass substrate was cleaned and loaded into a high vacuum (10^{-6} mbar) e-beam evaporator, and a 50 nm layer of Al was deposited at 1.0 Ås^{-1}. The substrate was removed from the evaporator and cleaned in an oxygen plasma (50 W, O_2 flow rate: 5 mL min^{-1}) for 5 min, before being immersed in a 5 mmol solution of ODPA in isopropanol (IPA) for 48 h. The coated substrate was then thermally annealed at 80 °C for 3 min in air, before rinsing lightly in IPA to remove unbound/residual SAM molecules. It was then returned to the e-beam evaporator for sequential deposition of an Al adhesion layer (5 nm, 1 Ås^{-1}) and an Au layer (45 nm, 1 Ås^{-1}). The substrate was removed from the evaporator, and after drying at 80 °C for 10 min on a hot plate, a ≈4-µm-thick PVDF layer was spin-cast on top of the Au layer from a heated solution (80 °C, 1000 rpm, 30 s). The coated substrate was then allowed to cool under ambient conditions for around three minutes to induce peeling of an Au/PVDF bilayer at the ODPA/Au interface. Note, 4 µm was empirically determined to be the minimum film thickness needed for reliable delamination of PVDF, with substantially thinner films of PVDF remaining adhered to the substrate.

Fabrication of Asymmetric Al/Au Electrodes: The procedure was the same as for the Al/ODPA/Au/PVDF coated substrates, except the Al was lithographically patterned in a concentric circle geometry prior to ODPA attachment, see Figure S5 in the Supporting Information. The lithographic patterning was carried out as follows: (a) aluminum was deposited using an e-beam evaporator across the entire glass substrate; (b) S1818 positive photoresist was deposited on top of the Al by spin-coating at 2000 rpm for 5 s and 5000 rpm for 35 s; (c) the resist was lightly baked at 115 °C for 1 min; (d) it was then selectively exposed at 405 nm (150 mJ cm^{-2}) via direct writing laser lithography (Heidelberg MLA 150); (e) the substrate was immersed in MF-726 developer (AZ electronics materials) for 90 s, rinsed and dried; (e) the Al was etched by immersion in Al etchant (ANPE80/5/5/10, Microchemicals) for about 30 s at 40 °C; (f) finally, the residual resist was removed by acetone and isopropanol, respectively.

Imaging: The morphology of PVDF under different thermal annealing conditions was studied by AFM (Veeco Metrology) using a QNM (Quantitative Nano Mechanical) mode with ScanAsyst air silicon tips. SEM images of the nanogap electrodes were obtained using an FEI APREO scanning electron microscope equipped with a field emission electron source and through-lens electron detectors. The electron-beam voltage and current conditions used for imaging were 5 kV and 13 pA, respectively.

Fabrication and Characterization of Devices: After fabrication of the asymmetric Al/Au nanogap electrodes by the procedure described above, the ODPA was removed by O_2 plasma ashing for a period of 5 min (50 W, O_2 flow rate: 5 mL min^{-1}). An active layer of P3HT (99.5%, Sigma-Aldrich) was then spin-cast onto the electrodes from a 5 mg mL^{-1} solution in chloroform at a speed of 2000 rpm for 40 s. The photodiodes were annealed in air at 120 °C for 6 min before measuring. Electrical contact was made to the devices using a probe station (Micromanipulators, Imina Technologies), before testing in air with a Keithley SCS 4202 parameter analyzer. Forward bias corresponds to the second deposited metal (M2) being positively biased with respect to the first deposited metal (M1). White light from the LED illumination source of a Nikon microscope (SMZ800, ≈20 mW cm^{-2}) was used to optically stimulate the full area of the photodiode. An equivalent procedure was followed for symmetric Al/Al nanogap devices.

Supporting Information

Supporting Information is available from the Wiley Online Library or from the author.

Acknowledgements

The experimental work was undertaken in the NTNU NanoLab with financial support from NTNU, project number 81617850. The Research Council of Norway is acknowledged for the support to the Norwegian Micro and Nano-Fabrication Facility, NorFab, project number 245963/F50.

Conflict of Interest

The authors declare no conflict of interest.

Keywords

adhesion, lithography, nanogap, self-peeling

Received: February 5, 2019
Revised: May 13, 2019
Published online:

[1] T. Li, W. Hu, D. Zhu, *Adv. Mater.* **2010**, *22*, 286.
[2] A. Cui, H. Dong, W. Hu, *Small* **2015**, *11*, 6115.
[3] X. Chen, Z. Guo, G.-M. Yang, J. Li, M.-Q. Li, J.-H. Liu, X.-J. Huang, *Mater. Today* **2010**, *13*, 28.
[4] V. Dubois, S. J. Bleiker, G. Stemme, F. Niklaus, *Adv. Mater.* **2018**, *30*, 1801124.

 © 2019 WILEY-VCH Verlag GmbH & Co. KGaA, Weinheim

[5] E. Lörtscher, B. Gotsmann, Y. Lee, L. Yu, C. Rettner, H. Riel, *ACS Nano* **2012**, *6*, 4931.
[6] V. Dubois, S. N. Raja, P. Gehring, S. Caneva, H. S. J. van der Zant, F. Niklaus, G. Stemme, *Nat. Commun.* **2018**, *9*, 3433.
[7] L. V. Brown, X. Yang, K. Zhao, B. Y. Zheng, P. Nordlander, N. J. Halas, *Nano Lett.* **2015**, *15*, 1272.
[8] V. R. Manfrinato, A. Stein, L. Zhang, C.-Y. Nam, K. G. Yager, E. A. Stach, C. T. Black, *Nano Lett.* **2017**, *17*, 4562.
[9] T. Miyazaki, K. Kobayashi, T. Horiuchi, H. Yamada, K. Matsushige, *Jpn. J. Appl. Phys.* **2001**, *40*, 4365.
[10] M. Fuechsle, J. A. Miwa, S. Mahapatra, H. Ryu, S. Lee, O. Warschkow, L. C. L. Hollenberg, G. Klimeck, M. Y. Simmons, *Nat. Nanotechnol.* **2012**, *7*, 242.
[11] R. Garcia, A. W. Knoll, E. Riedo, *Nat. Nanotechnol.* **2014**, *9*, 577.
[12] H. Choo, M. K. Kim, M. Staffaroni, T. J. Seok, J. Bokor, S. Cabrini, P. J. Schuck, M. C. Wu, E. Yablonovitch, *Nat. Photonics* **2012**, *6*, 838.
[13] A. Cui, Z. Liu, H. Dong, Y. Wang, Y. Zhen, W. Li, J. Li, C. Gu, W. Hu, *Adv. Mater.* **2015**, *27*, 3002.
[14] L. Qin, S. Park, L. Huang, C. A. Mirkin, *Science* **2005**, *309*, 113.
[15] T. Ozel, G. R. Bourret, C. A. Mirkin, *Nat. Nanotechnol.* **2015**, *10*, 319.
[16] J. Park, A. N. Pasupathy, J. I. Goldsmith, C. Chang, Y. Yaish, J. R. Petta, M. Rinkoski, J. P. Sethna, H. D. Abruña, P. L. McEuen, D. C. Ralph, *Nature* **2002**, *417*, 722.
[17] B. Lam, W. Zhou, S. O. Kelley, E. H. Sargent, *Nat. Commun.* **2015**, *6*, 1.
[18] A. R. Madaria, M. Yao, C. Chi, N. Huang, C. Lin, R. Li, M. L. Povinelli, P. D. Dapkus, C. Zhou, *Nano Lett.* **2012**, *12*, 2839.
[19] H. Im, K. C. Bantz, S. H. Lee, T. W. Johnson, C. L. Haynes, S. H. Oh, *Adv. Mater.* **2013**, *25*, 2678.
[20] X. Chen, H. R. Park, M. Pelton, X. Piao, N. C. Lindquist, H. Im, Y. J. Kim, J. S. Ahn, K. J. Ahn, N. Park, D. S. Kim, S. H. Oh, *Nat. Commun.* **2013**, *4*, 1.
[21] D. Yoo, K. L. Gurunatha, H. K. Choi, D. A. Mohr, C. T. Ertsgaard, R. Gordon, S. H. Oh, *Nano Lett.* **2018**, *18*, 3637.
[22] L. Sun, Y. A. Diaz-Fernandez, T. A. Gschneidtner, F. Westerlund, S. Lara-Avila, K. Moth-Poulsen, *Chem. Soc. Rev.* **2014**, *43*, 7378.
[23] Z. Zhou, Z. Zhao, Y. Yu, B. Ai, H. Möhwald, R. C. Chiechi, J. K. W. Yang, G. Zhang, *Adv. Mater.* **2016**, *28*, 2956.
[24] D. J. Beesley, J. Semple, L. Krishnan Jagadamma, A. Amassian, M. A. McLachlan, T. D. Anthopoulos, J. C. Demello, *Nat. Commun.* **2014**, *5*, 1.
[25] G. Wyatt-Moon, D. G. Georgiadou, A. Zoladek-Lemanczyk, F. A. Castro, T. D. Anthopoulos, *J. Phys.: Mater.* **2018**, *1*, 01LT01.
[26] G. Wyatt-Moon, D. G. Georgiadou, J. Semple, T. D. Anthopoulos, *ACS Appl. Mater. Interfaces* **2017**, *9*, 41965.
[27] J. Semple, S. Rossbauer, T. D. Anthopoulos, *ACS Appl. Mater. Interfaces* **2016**, *8*, 23167.
[28] J. Semple, S. Rossbauer, C. H. Burgess, K. Zhao, L. K. Jagadamma, A. Amassian, M. A. McLachlan, T. D. Anthopoulos, *Small* **2016**, *12*, 1993.
[29] T. Kawanago, S. Oda, *Appl. Phys. Lett.* **2017**, *110*, 133507.
[30] J. Semple, D. G. Georgiadou, G. Wyatt-Moon, M. Yoon, A. Seitkhan, E. Yengel, S. Rossbauer, F. Bottacchi, M. A. McLachlan, D. D. C. Bradley, T. D. Anthopoulos, *npj Flexible Electron.* **2018**, *2*, 18.
[31] J. Semple, G. Wyatt-Moon, D. G. Georgiadou, M. A. McLachlan, T. D. Anthopoulos, *IEEE Trans. Electron Devices* **2017**, *64*, 1973.
[32] S. G. Croll, *J. Coat. Technol.* **1980**, *52*, 35.
[33] Y. Tai, G. Lubineau, *Adv. Sci.* **2017**, *4*, 1.
[34] H. Zhu, T. Li, Y. Zhang, H. Dong, J. Song, H. Zhao, Z. Wei, W. Xu, W. Hu, Z. Bo, *Adv. Mater.* **2010**, *22*, 1645.
[35] S. Pang, S. Yang, X. Feng, K. Müllen, *Adv. Mater.* **2012**, *24*, 1566.
[36] P. Gu, W. Zhang, G. Zhang, *Adv. Mater. Interfaces* **2018**, *5*, 1800648.
[37] J. Yang, J. You, C.-C. Chen, W.-C. Hsu, H. Tan, X. W. Zhang, Z. Hong, Y. Yang, *ACS Nano* **2011**, *5*, 6210.
[38] The slight asymmetry in the I–V characteristics of the symmetric device suggests a small difference in the work functions of the two Al electrodes due to different deposition/processing conditions, resulting in easier carrier injection when M2 is biased positively with respect to M1. The comparatively weak PV response is partly attributable to the use of the same metal for anode and cathode, which results in a low built-in field. It may also be the case that the use of a noble-metal (gold) electrode in the asymmetric device causes a substantial increase in light absorption due to near-field enhancement at the nanogap,[36,37] resulting in much higher photocurrents than for the Al/P3HT/Al device.

© 2019 WILEY-VCH Verlag GmbH & Co. KGaA, Weinheim